Solid Earth Discuss., 5, 281–314, 2013
www.solid-earth-discuss.net/5/281/2013/
doi:10.5194/sed-5-281-2013

Solid Earth
Discussions
Open Access

Short wavelength undulatory extinction in quartz recording coseismic deformation in the middle crust – an experimental study

C. A. Trepmann[1] and B. Stöckhert[2]

[1]Department for Earth and Environmental Sciences, Ludwig-Maximilians-Universität München, Germany
[2]Institute of Geology, Mineralogy and Geophysics, Ruhr-Universität Bochum, Germany

Received: 20 March 2013 – Accepted: 21 March 2013 – Published: 8 April 2013

Correspondence to: C. A. Trepmann (claudia.trepmann@lmu.de)

Published by Copernicus Publications on behalf of the European Geosciences Union.

Abstract

Deformation experiments are carried out on natural vein quartz in a modified Griggs-type solid medium apparatus to explore the preservation potential of microfabrics created by crystal-plastic deformation at high stress, overprinted during subsequent creep at lower stress. a corresponding stress history is expected for the upper plastosphere, where fault slip during an earthquake causes quasi-instantaneous loading to high stress, followed by stress relaxation. The question is whether evidence of crystal-plastic deformation at high stress, hence an indicator of past seismic activity, can still be identified in the microstructure after overprint by creep at lower stresses. Firstly, quartz samples are deformed at a temperature of 400 °C and constant strain rate of $10^{-4}\,s^{-1}$ ("kick"), and then held at 900 to 1000 °C at residual stress ("creep"). In quartz exclusively subject to high-stress deformation, lamellar domains of slightly differing crystallographic orientation (misorientation angle $< 2°$) and a few tens of micrometers wide occur. In transmission electron microscope (TEM), these areas show a high density of tangled dislocations and cellular structures. After "kick and creep" experiments, pronounced short-wavelength undulatory extinction (SWUE) is observed in the optical microscope. The wavelength of SWUE is up to 10 µm, with oscillatory misorientation of up to a few degrees. TEM inspection reveals domains with high density of dislocations and differing diffraction contrast bound by poorly-ordered dislocation walls. Only zones with exceptional damage generated during high-stress deformation are replaced by small new grains with a diameter of about 10 to 20 µm, forming strings of recrystallized grains. For large original grains showing SWUE, the Schmid factor for basal ⟨a⟩ glide is found to be high. SWUE is taken to reflect high-stress crystal-plastic deformation, the modified microstructure being sufficiently stable to be recognized after subsequent creep as an indicator of past seismic activity.

SED
5, 281–314, 2013

1 Introduction

Seismic activity in the upper crust implies a cyclic stress history in the lower crust (e.g. Tse and Rice, 1986; Ben-Zion and Rice, 1997; Ben-Zion and Lyakhovsky, 2006; Ellis and Stöckhert, 2004; Nüchter and Ellis, 2010). During a large earthquake (Scholz, 2002), coseismic stress relief in the schizosphere is concomitant with quasi-instantaneous loading in the underlying plastosphere, (Fig. 1). Inversely, slow stress relaxation by creep in the deeper crust is concomitant with gradual reloading of the brittle fault above. The terms schizosphere and plastosphere were introduced by Scholz (2002). Schizosphere denotes the layer transected by coseismic rupture during a large earthquake. Rupture does not propagate into the underlying plastosphere. The boundary between these spheres is defined for the instant of a large earthquake only (Fig. 1). It lies at greater depth compared to the long-term brittle-viscous transition, which – for continental crust – is commonly associated with the onset of slow deformation by dislocation creep of quartz at temperatures around 300 °C (e.g. Dunlap et al., 1997; Stöckhert et al., 1999; van Daalen, 1999; Hirth et al., 2001; Stipp et al., 2002). The seismogenic zone, where earthquakes nucleate along brittle faults, is confined to within the schizosphere (e.g. Scholz, 2002; Ben-Zion, 2008).

The effects of earthquake-related stress cycles in the deeper crust, with quasi-instantaneous loading leading to brittle and crystal-plastic deformation followed by a stage of creep at decaying stress, are identified in the record of exhumed metamorphic rocks. They are most pronounced in the uppermost plastosphere (e.g. Küster and Stöckhert, 1999; Trepmann and Stöckhert, 2001, 2002, 2003). The natural microstructures provide insight in details of deformation processes on microscopic scale, taking place at depths not accessible for in situ observation. Drawback is the necessity to decipher a fossil record not being quenched, but progressively re-shaped in successive episodes at differing conditions throughout geologic history – a demanding situation.

Laboratory experiments can be designed to simulate coseismic loading to high stress in the uppermost plastosphere. For this stage of rapid loading, conditions in terms of

SED
5, 281–314, 2013

strain rate and stresses attained come close to those expected for natural deformation (Trepmann et al., 2007; Druiventak et al., 2012). Consequently, microfabrics developed in these experiments are expected to correspond to those formed in nature. Unfortunately, a direct comparison is precluded by the prolonged cooling history of metamorphic rocks exhumed over millions of years. During that part of the history, microfabrics developed at coseismic loading are progressively modified in the later course of the same cycle by creep at decaying stress. Moreover, overprinting of repeated cycles is very likely, blurring the original record.

To establish evidence for ancient stress cycles in the middle crust, induced by large earthquakes in the overlying schizosphere, it is necessary to identify microstructural indications of rapid coseismic loading to high stress, despite being necessarily overprinted during a prolonged period of creep during stress relaxation. In natural rocks, indicators for short term deformation are for instance mechanical twinning (Trepmann and Stöckhert, 2001) or multiple fragmentation of strong brittle crystals embedded in a ductile matrix (Trepmann and Stöckhert, 2002; Le et al., 2005). In these cases, resulting characteristic microstructures are not destroyed by subsequent creep. For quartz the situation is more complicated, as microstructures created during quasi-instantaneous loading at temperatures above about 300 °C are modified or entirely obliterated in the course of subsequent creep during stress relaxation (Trepmann and Stöckhert, 2003). Laboratory experiments designed to explore the effects of such overprint require high temperatures, in order to speed up processes and to keep stresses at a level expected for nature.

To explore microstructures bearing potential for identification of an initial high-stress deformation event in rocks with a subsequent prolonged creep history, a set of experiments combining high-stress and low-stress deformation on natural vein quartz are performed. We follow the original concept of “kick and cook” experiments, designed to simulate coseismic loading and postseismic annealing in the uppermost plastosphere (Trepmann et al., 2007; Druiventak et al., 2011, 2012). In this study, we replace the “cook” procedure, which denotes a stage of high temperature and nominally zero

SED
5, 281–314, 2013

differential stress, by a more realistic "creep" stage at high temperature and moderate residual stress, during which microstructures created in the initial stage of high-stress deformation ("kick") become modified during further deformation. Microstructures created in "kick and creep" experiments in the laboratory are expected to represent the record of quartz acquired in the uppermost plastosphere in tectonically active regions of continental crust, and are probably preserved in many exhumed metamorphic rocks due to contemporary cooling. The goal is to identify microstructures still preserving evidence for an earlier coseismic stress peak, despite being modified during subsequent creep deformation at lower stress.

2 Experimental strategy

Triaxial deformation experiments on natural vein quartz were performed in a modified Griggs-type, servohydraulically controlled, solid-medium deformation apparatus (Rybacki et al., 1998). Starting material is pure natural vein quartz (CR1; > 99.9 % quartz) with grain size of ~ 1 mm and average dislocation density on the order of $10^{12}\,m^{-2}$, as described by Trepmann et al. (2007). Cylindrical samples with a length of ~ 7 mm and a diameter of ~ 3.3 mm are prepared by drilling. Platinum capsules are used with a wall thickness of 0.1 mm to prevent reaction between specimen and the surrounding pressure transmitting medium, which is a mixture of 65.5 mole% CsCl and 34.5 mole% NaCl. Heating is provided by a graphite resistance furnace and temperature is measured by two thermocouples, placed close to the upper and lower end of the sample, respectively. The axial piston movement is controlled using the signal of two displacement transducers.

The initial stage of high-stress deformation ("kick") is performed at a temperature of 400 °C and a confining pressure of 2.0 GPa. The axial force is increased up to 60–80 kN by propagating the axial piston into the sample assembly with a constant velocity of 2.5–2.9 mm h^{-1}, corresponding to a strain rate of about $10^{-4}\,s^{-1}$ for a sample length of 7–8 mm. For the subsequent stage of low-stress deformation ("creep"), the axial

SED
5, 281–314, 2013

piston is first retracted to reduce remaining load on the sample to about 50 kN. Afterwards, temperature is raised to between 900 °C and 1000 °C at confining pressure of 2.5 or 2.7 GPa (Table 1), the conditions being held for 16 h. With respect to axial load, two different types of run are performed (Fig. 2). In experiment CR1-13, the axial piston is advanced into the sample assembly with a rate of 0.07 mm h^{-1}, keeping the load approximately constant. In experiments CR1-14 through CR1-17, the axial piston remains stationary and axial load decreases with time during creep deformation.

Temperature applied in "kick" experiments is similar to that expected in the upper plastosphere of continental crust, where coseismic stress changes during major earthquakes lead to quasi-instantaneous deformation. For the sake of a well controlled experiment and protection of apparatus, strain rate is chosen somewhat lower compared to that expected for coseismic deformation, while confining pressure $\sigma_2 = \sigma_3 = 2$ GPa exceeds expected natural conditions by a factor of > 4, which helps to suppress brittle failure. For the subsequent "creep" experiment, confining pressure is further increased in order to keep experimental conditions in the stability field of α-quartz and to prevent melting of confining medium. The "creep" experiment is designed to represent postseismic creep in the uppermost plastosphere. Temperatures of 900–1000 °C are required to speed up creep deformation accompanied by recovery and recrystallization, which otherwise would not be accessible on laboratory time scales. The trade temperature for rate is commonplace in experimental rock deformation, being the only way to achieve measurable deformation at stress levels corresponding to those prevailing in nature (e.g. Paterson, 1987, 1990; Evans and Kohlstedt, 1995). For pure quartz aggregates, experimental deformation at high temperatures and high strain rates was demonstrated to yield microfabrics similar to natural rocks (e.g. Stöckhert et al., 1999; Hirth and Tullis 1992, 1994; Hirth et al., 2001; Stipp et al., 2002; Stipp and Tullis, 2003).

SED
5, 281–314, 2013

3 Analytical methods

Polished thin sections (~ 30 µm) were prepared from the experimentally deformed samples, cut parallel to the cylinder axis, and used for microstructural analysis by optical and scanning electron microscopy (SEM). Crystallographic orientation and microfabric of quartz were analysed by electron backscatter diffraction (EBSD) using a LEO 1530 scanning electron microscope. For indexing and processing of the data, the Oxford Instruments HKL software *CHANNEL 5* was used. Crystallographic preferred orientations (CPO) are displayed as stereographic projections of the lower hemisphere.

Arrangement and density of dislocations in quartz were examined by transmission electron microscopy (TEM), using a Philips EM301 transmission electron microscope operated at 100 kV. TEM foils were prepared by focussed ion beam (FIB) technique with a FEI Quanta200 3-D instrument. All diffraction contrast images were obtained at bright field conditions. Dislocation densities ρ are derived from TEM micrographs by counting the number of dislocation lines (N) intersecting a unit area (A) with $\rho = 2N/A$ (Karato, 2008).

4 Mechanical data

For the high-stress deformation ("kick") experiment, force-displacement data were transformed into stress-strain curves, applying corrections for friction between axial piston and parts of the sample assemblage, as described by Trepmann et al. (2007). After reaching the elastic limit, stress increases with increasing strain in a non-linear manner, reflecting inelastic deformation with work hardening. Distinct stress drops are not observed. Maximum differential stress attained in the experiments is between 1.2 and 3.5 GPa. According to the stress-strain curves (Table 1), axial strain (ε_1) accumulated during the "kick" stage of the experiments remains well below 3 %. The total sample strain (ε_{tot}) attained after "kick and creep" experiments is determined by comparing the length of the quartz cylinder before and after deformation. It amounts to between 1.4

SED
5, 281–314, 2013

and 6.5 % (Table 1) for experiments CR1-14 through CR1-17 with stress relaxation, and 13 % for experiment CR1-13, where the piston was advanced slowly (0.07 mm h^{-1}) into the sample assembly holding the stress level approximately constant. Cracks perpendicular to the cylinder axis resulting from unloading (e.g. Tonge et al., 2012) transect the entire sample and cause underestimation of total sample strain. For the "creep" stage, approximate strain rates are estimated by dividing strain ($\varepsilon_{tot} - \varepsilon_1$) by duration. One obtains strain rates between 0.2 and 1.8 × 10^{-6} s^{-1} (Table 1). As correction for friction, comparable to that used for the "kick" stage (Fig. 2), is not possible for the creep stage, reliable estimates of residual stress driving deformation cannot be derived from stress-strain curves. Instead, differential stress is estimated from strain rate, using an experimental flow law for dislocation creep of quartz (Paterson and Luan, 1990). For given temperatures of 900 to 1000 °C and strain rates on the order of 10^{-6} s^{-1}, inferred differential stress effective during the "creep" stage is about 125 to 250 MPa. In experiments CR1-14 through CR1-17, stresses decayed in the course of the experiment and the derived strain rates of 0.2 to 1.1 × 10^{-6} s^{-1} represent average values. Consequently, in "creep" experiments CR1-14 through CR1-17 differential stresses initially exceeded the nominal values of 125 to 150 MPa, and may have been similar to 250 MPa as obtained for experiment CR1-13 (Table 1).

5 Microfabrics

The microstructures observed after "kick" experiments serve as reference for overprint during the following creep stage in "kick and creep" experiments (Table 1). After the "kick" experiment, the samples show arrays of microcracks (Fig. 3). The length of the individual microcracks is typically about 50 µm, their spacing about 25 µm and they are oriented normal to the cylinder axis, i.e. normal to the major principal stress σ_1 during deformation. Given this orientation, which is the same as for the cracks crosscutting the entire sample, they are likewise interpreted to result from unloading (e.g. Tonge et al., 2012). In contrast, these microcrack arrays are associated with domains that reveal a

SED
5, 281–314, 2013

slight misorientation < 2° with respect to the intact host, visible by slightly differing extinction in the polarization microscope, and confirmed by EBSD (Fig. 3). The change in crystallographic orientation is not progressive, as would be expected for overall bending of the crystal, but oscillating (Fig. 3b, d). Although relative misorientation revealed in the EBSD profile (Fig. 3d) barely emerges from noise, the map displayed in Fig. 3b reveals that misorientation corresponds to the optically visible features. The domain boundaries are aligned approximately parallel to the (0001) plane of quartz (Fig. 3a). Within the domains shown in Fig. 3a, tiny lamellae with a spacing of a few µm are oriented apparently parallel to {z} rhombohedral planes, as indicated by the combination of polarization microscopy and EBSD-data. a second set of slightly more diffuse and wider lamellae with a wider spacing of about 15 µm are apparently parallel to {r} rhombohedral planes. On the TEM scale, areas with these characteristic microcrack arrays and lamellar structures show a high density of tangled dislocations and domains of lower dislocation density (Fig. 4), resembling a cellular structure known from cold worked materials (e.g. Humphreys and Hatherly, 2004).

After "kick and creep" experiments with low total strain of < 10 % (stationary piston during "creep", Table 1), the optical microstructure is characterized by (1) pronounced short-wavelength undulatory extinction (SWUE), (2) distinct deformation bands, and (3) occurrence of new grains aligned along strings at variable angle to shortening direction (Figs. 5–7). Quartz grains showing SWUE appear crinkly with narrow bands oscillating in crystallographic orientation. Misorientation angles are up to about 2° (Figs. 5c, f, 6b, d). Spacing of these bands corresponds to their width, showing a wavelength of 10 to 20 µm (Fig. 7a, b). In contrast to SWUE, distinct deformation bands are characterized by plane and subparallel boundaries, and by a higher misorientation angle of about 10–15° (Fig. 6a, b, d). Their orientation appears to be parallel to prism planes. The diameter of new recrystallized grains aligned in strings is about 10 to 30 µm, as indicated by a combination of polarization microscopy and EBSD observations (Fig. 7b–d). Some isolated grains situated along deformation bands have a roughly rectangular grain shape and a larger diameter of 50–200 µm (Fig. 5b). The

SED
5, 281–314, 2013

orientation of new grains is nearly random but can locally show some orientation relation to the deformed host (Fig. 7b–d). The proportion of recrystallized grains is highly variable due to inhomogeneous deformation, reaching up to about 10 % in samples CR1-14 through CR1-17, with moderate creep strain up to a few percent. For sample CR1-13, with creep strain of > 10 % (Table 1), recrystallized grains with a grain diameter of 20–30 µm cover an area of about 40 %, being inhomogeneously distributed (Fig. 8). Large relict grains with a high Schmid factor for basal ⟨a⟩ glide reveal well-developed SWUE (Fig. 8b, c). Here, the orientation of SWUE is subparalel to {m} prism planes (Fig. 8b). Recrystallized grains show a weak CPO, which is controlled by the crystallographic orientation of the remnant grains (Fig. 8e). Two of the {r} rhombohedral planes are oriented preferentially in a plane perpendicular to the shortening direction, whereas the other {r} rhombohedral plane is oriented parallel to the shortening direction, corresponding to the easy glide position for basal ⟨a⟩ glide (Fig. 8e). In places, recrystallized grains show shape preferred orientation (SPO) with the long axes oriented in a plane perpendicular to the shortening direction (Fig. 8f).

In samples subject to "kick and creep" experiments, areas of quartz showing SWUE are characterized by dislocation densities on the order of 10^{12} to 10^{13} m^{-2} (Fig. 9). Dislocations are less tangled compared to "kick" experiments, but instead arranged in poorly-ordered dislocation walls, separating domains with different diffraction contrast (Fig. 9a, b). These walls are lined up parallel to the optically visible deformation lamellae. In contrast, in recrystallized new grains dislocation density is very low (Fig. 9d).

6 Discussion

6.1 Low-temperature plasticity

According to the empirical Goetze's criterium (Evans and Kohlstedt, 1995), a material is expected to deform entirely by crystal-plastic mechanisms, when confining pressure exceeds differential stress. In the course of "kick" experiments carried out at a confining

SED
5, 281–314, 2013

pressure of 2 GPa, differential stress is observed to increase to > 2 GPa during progressive deformation (Fig. 2), with the exception of experiment CR1-15 (Table 1). After initial glide-controlled deformation in the low-temperature plasticity regime, limited by strain hardening, the field of semi-brittle deformation is probably entered. For the earlier stage of deformation with strain hardening (Fig. 2), crystal-plastic deformation of quartz is expected to predominate at temperatures of 400 °C and strain rates of 10^{-4} s^{-1}.

In the low-temperature plasticity field, crystal-plastic deformation of quartz is characteristically inhomogeneous, due to limited number of activated glide systems (e.g. Paterson, 1969; Nicolas and Poirier, 1976; Paterson and Wong, 2005). In the polarization microscope, inhomogeneous deformation is reflected by undulatory extinction, domains with low oscillatory misorientation, and deformation lamellae, reflecting the presence of geometrically necessary dislocations (Nicolas and Poirier, 1976). On the TEM-scale, high density of tangled dislocations and cellular structure (Fig. 4) is commonly observed after glide-controlled deformation in the low-temperature plasticity regime for various materials (e.g. Tsenn and Carter, 1987; Fredrich et al., 1989; Humphreys and Hatherly, 2004; Druiventak et al., 2011) including quartz (Carter et al., 1981; Hirth and Tullis, 1994). Tangled dislocations imply that glide becomes increasingly inhibited, giving rise to work hardening (e.g. Nicolas and Poirier, 1976; Humphreys and Hatherly, 2004; Durinck, et al., 2007) as observed for "kick" experiments (Fig. 3).

The domains with microcrack arrays up to about 50 µm wide formed in "kick" experiments show boundaries perpendicular to the c-axis, parallel to the (0001) plane of quartz (Fig. 3), comparable to commonly observed sub-basal deformation lamellae in quartz (e.g. McLaren et al., 1970; McLaren and Hobbs, 1972; White, 1973, 1975; Christie and Ardell, 1974; Drury, 1993). Also, the characteristic oscillating microstructure with misorientation angles of < 2° and the high density of tangled dislocations (Fig. 3) are similar. The sets of parallel microcracks confined to these domains (Fig. 3b) demonstrate, that brittle failure is controlled by preceding crystal-plastic deformation. The tensile microcracks being oriented normal to the cylinder axis, i.e. normal to the maximum principal stress during the "kick" experiment, indicates that brittle fail-

SED
5, 281–314, 2013

ure occurred during unloading. Nucleation of cracks is expected to be facilitated in regions that previously underwent strain hardening by pile up of dislocations.

Similar deformation lamellae in olivine were observed by Druiventak et al. (2011) to form in deformation experiments at 600 °C on natural peridotites. In olivine, these lamellae are parallel to (100) and are associated with a high density of [001] screw dislocations. After deformation experiments at 300 °C, instead fractures parallel (100) are observed with similar spacing as the deformation lamellae produced at 600 °C. The fractures were interpreted by Druiventak et al. (2011) to have developed as a consequence of hardening by pile up of dislocations, whereas at 600 °C crystal plastic deformation was more effective and stress concentration did not lead to brittle failure.

Within these sub-basal domains, two sets of narrow lamellae with slight misorientation are visible on optical scale, oriented parallel to {r} and {z} rhombohedral planes. At low temperatures, the critical resolved shear stress for activation of ⟨a⟩ glide on rhombohedral planes exceeds that for basal ⟨a⟩ glide (Hobbs, 1968, 1985; Schmid and Casey, 1986; Kruhl, 1996; Heilbronner and Tullis, 2002). The optical microstructures with sub-basal domains hosting lamellae parallel to {r} and {z} rhombohedral planes suggests that differential stress attained during "kick" deformation was sufficient for simultaneous activation of both basal ⟨a⟩ and rhomb ⟨a⟩ glide systems.

6.2 Short wavelength undulatory extinction – SWUE

After "kick and creep" experiments, the microstructure is different from that developed after "kick" experiments. Microstructures reflecting deformation in the low-temperature plasticity field at high differential stress are modified by thermally activated processes taking place during the "creep" experiment. After experiments with fixed axial piston and decaying stress during "creep", resulting in a total strain < 10 % (Figs. 5–7), SWUE is the prominent microstructural feature within preserved original grains discernible under the polarization microscope.

The appearance of SWUE differs in geometry and orientation from that of sub-basal deformation lamellae in quartz described by, e.g. McLaren et al. (1970), McLaren and

SED
5, 281–314, 2013

Hobbs (1972), White (1973, 1975), Christie and Ardell (1974), and Drury (1993), although the characteristic oscillating microstructure with misorientation angles of at best a few degrees is similar. Previous TEM investigations revealed that several submicroscopic structures can be associated with sub-basal deformation lamellae visible on optical scale. The lamellae can be defined by arrays of elongate subgrains (McLaren and Hobbs, 1972; White, 1973; Blenkinsop and Drury, 1988; Drury, 1993; Trepmann and Stöckhert, 2003), bands of variable dislocation density, and planar arrays of fluid inclusions indicating crack healing (White, 1973, 1975; Christie and Ardell, 1974; White and Treagus, 1975; Drury, 1993) or localized precipitation of an aqueous phase (Wilkins and Barkas, 1978). Sub-basal deformation lamellae in quartz have been proposed to reflect glide-controlled deformation combined with dynamic recovery (McLaren and Hobbs, 1972; McLaren, 1991; Drury, 1993; Trepmann and Stöckhert, 2003; Vernooij and Langenhorst, 2005), being comparable with similar lamellae observed in metal alloys (Drury and Humphreys, 1986, 1987).

SWUE as observed here (Figs. 5–8, 11), has evolved by dynamic recovery during "creep" experiments from areas with a high defect density and tangled dislocation (Fig. 4), which had been produced by glide-controlled deformation in the low-temperature plasticity regime in the preceding "kick" experiment. The overprint results in SWUE with lamellar spacing on the order of 0.01 mm and small oscillatory misorientation. In contrast, a pronounced SWUE in quartz was not observed in previous "kick and cook" experiments, which denotes high-stress deformation followed by isostatic annealing (Trepmann et al., 2007). This implies that SWUE is not produced during climb-controlled static recovery, but requires ongoing deformation including multiplication of dislocations and dynamic recovery.

Deformation bands parallel to prism planes are consistent with basal ⟨a⟩ glide predominating during creep (Fig. 6). Individual bands and lamellae are bound by less tangled dislocations, compared to microstructure developed after "kick" experiments, and dislocation walls including a share of geometrically necessary dislocations required for misorientation. As low-angle grain boundaries, such configurations are rather

SED
5, 281–314, 2013

stationary and not prone to migration (Humphreys and Hatherly, 2004), spacing and misorientation being preserved while TEM-scale microstructure is undergoing modification.

6.3 Recrystallization

Recrystallization is concurrent to recovery. During deformation at high temperatures, or during static annealing, both processes reducing dislocation density proceed side by side (e.g. Cotterill and Mould, 1976; Poirier, 1985; Humphreys and Hatherly, 2004). Recrystallization by formation and migration of high-angle grain boundaries seems to be more effective in highly strained zones, whereas recovery predominates elsewhere (e.g. Fitz Gerald and Stünitz, 1993; Trimby et al., 1998; Passchier and Trouw, 2008; Stipp and Kunze, 2008; Druiventak et al., 2012). Accordingly, zones of intense crystal-plastic deformation resulting from the "kick" experiment are replaced by small new grains during the "creep" experiment. These new grains are typically 10 to 20 µm in diameter, forming strings of recrystallized grains, similar to those observed after the "kick and cook" experiments by Trepmann et al. (2007). In that earlier study, growth of new grains was inferred to have started from crystallites poor in dislocations, which had been formed by brittle comminution along cracks generated during the "kick" experiment. This interpretation is based on the observation that the new grains display a nearly random crystallographic orientation, in most cases not related to the orientation of the deformed parental quartz. Reorientation of these small crystallites is envisaged to take place by rotation of tiny fragments along shear fractures, followed by formation and migration of mobile high-angle grain boundaries with high misorientation. Here, also a cellular structure characterized by defect-poor domains embedded in surroundings of high dislocation density are observed in deformed samples (Fig. 4b). Cells with high misorientation may act as seeds for the formation of new grains. Similar recrystallization microfabrics are described for olivine deformed in "kick and cook" experiments on peridotites (Druiventak et al., 2012).

SED
5, 281–314, 2013

Whether old grains deformed in the "kick" experiment are replaced by new grains, or their internal structure resulting from inhomogeneous deformation evolves into SWUE by dynamic recovery, depends on strain accumulated during initial high-stress deformation. Where strain was concentrated, i.e. at sites where local brittle grain comminution occurred or at sites of extremely high dislocation densities, new grains developed. In contrast, in areas of lower strain, dynamic recovery results in SWUE.

In "creep" experiment CR1-13, where the axial piston is further advanced into the sample assembly, with deformation at persistent differential stresses of about 250 MPa and accumulated strain of about 13 %, the original coarse-grained quartz is largely recrystallized. Preserved large original in between recrystallized grains commonly have a high Schmid factor for basal ⟨a⟩ glide, and these grains show well-developed SWUE (Fig. 8a, b). Whereas dislocation density in grains with SWUE is still as high as 10^{12} to 10^{13} m^{-2}, new grains show a very low dislocation density.

6.4 Implications and comparison to natural microstructures

Whereas deformation bands can develop during continuous deformation by dislocation creep with dynamic recovery, gradually increasing misorientation, SWUE requires a preceding stage of deformation at high stress in the low-temperature plasticity regime. Accordingly, SWUE is interpreted to be characteristic for a sequence of (1) high-stress deformation with strain hardening, pile up of dislocations, formation of cell-structures, and locally brittle failure (as in experiments CR1-1 and CR1-3), and subsequent (2) creep at decaying stress with dynamic recovery (experiments CR1-14 to CR1-17). The generation of SWUE requires that only small strain was accumulated during both stages (1) and (2), for stage (1) probably limited by work hardening. If higher strain is accumulated during "creep", as in experiment CR1-13 (Table 1), recrystallization becomes more effective and eliminates old grains.

In preserved old grains, SWUE is a sufficiently stable microstructure to keep the record of an earlier stage of deformation in the low-temperature plasticity regime, followed by dislocation creep at lower stress. As such, SWUE represents a valuable

SED
5, 281–314, 2013

indicator for past seismic activity and stress cycles affecting the uppermost plastosphere. Moreover, SWUE suggests that stress relaxation was sufficiently fast to prevent prolonged creep with dynamic recrystallization, as otherwise respective grains would have been eliminated by recrystallization.

In natural rocks, pronounced SWUE has been observed in vein quartz from various localities, e.g. from St. Paul la Roche (Fig. 10, Trepmann, 2009), from Rugsundøya, Norway (Birtel and Stöckhert, 2008, their Fig. 7d) and from Evia, Greece (Nüchter and Stöckhert, 2007a, their Fig. 11e). Also, microstructures resembling SWUE in experimentally deformed quartz have been described in naturally deformed olivine from the Balmuccia peridotite complex, (Matysiak and Trepmann, 2012, their Figs. 6d, 7a). These natural quartz and olivine microstructures occur in samples, where microstructures are independently interpreted to reflect coseismic loading and postseismic stress relaxation in the uppermost plastosphere, near the lower tip of a seismically active fault.

7 Summary and conclusions

The main findings of our experiments are:

1. Deformation of quartz in the low-temperature plasticity regime at high stress ("kick") results in broad domains and different sets of narrow lamellae, with misorientation angles $< 2^{\circ}$ (Fig. 3). On TEM-scale, these regions are characterized by a high density of tangled dislocations and a cellular structure (Fig. 4). Such microfabrics will not be observed in naturally deformed rocks, as they are modified during a prolonged cooling history.

2. During subsequent deformation at lower stress, these features evolve to a pronounced short-wavelength undulatory extinction (SWUE) by creep with dynamic recovery.

3. Shear zones with high strain accumulated during "kick" experiments are replaced by strings of recrystallized grains with a diameter of about 10–20 µm.

SED
5, 281–314, 2013

4. Prolonged creep at approximately constant stress increases the volume proportion of recrystallized grains. Large preserved original grains display a high Schmid factor for basal ⟨a⟩ glide and well-developed SWUE.

5. SWUE in quartz is proposed to represent a stable microfabric indicative of a stage of crystal plastic deformation at high stress, which is sufficiently stable to be recognized in rocks with a prolonged subsequent creep deformation history.

6. As such, SWUE is proposed to record a cyclic stress history in the uppermost plastosphere, related to past large earthquakes.

Acknowledgements. This study has been funded by the DFG-Collaborative Research Centre 526.

References

Ben-Zion, Y. and Lyakhovsky, V.: Analysis of aftershocks in a lithospheric model with seismogenic zone governed by damage rheology, Geophys. J. Int., 165, 197–210, 2006.

Birtel, S. and Stöckhert, B.: Quartz veins record earthquake-related brittle failure and short term ductile flow in the deep crust, Tectonophysics, 457, 53–63, 2008.

Blenkinsop, T. G. and Drury, M. R.: Stress estimates and fault history from quartz microstructures, J. Struct. Geol., 10, 673–684, 1988.

Carter, N. L., Anderson, D. A., Hansen, F. D., and Kranz, R. L.: Creep and creep rupture of granitic rocks, Geoph. Monog. Series, 24, 61–82, 1981.

Christie, J. M. and Ardell, A. J.: Substructures of deformation lamellae in quartz, Geology, 2, 405–408, 1974.

Druiventak, A., Trepmann, C. A., Renner, J., and Hanke, K.: Low-temperature plasticity of olivine during high stress deformation of peridotite at lithospheric conditions – an experimental study, Earth Planet. Sc. Lett., 311, 199–211, doi:10.1016/j.epsl.2011.09.022, 2011.

Druiventak, A., Matysiak, A., Renner, J., and Trepmann, C. A.: Kick-and-cook experiments on peridotite: simulating coseismic deformation and post-seismic creep, Terra Nova, 24, 62–69, 2012.

SED
5, 281–314, 2013

Drury, M. R.: Deformation lamellae in metals and minerals, in: Defects and Processes in the Solid State, Geoscience Applications, the McLaren Volume, edited by: Boland, J. N., Fitzgerald, J. D., 195–212, 1993.
Drury, M. R. and Humphreys, F. J.: The development of microstructures in Al-5 % Mg during high temperature deformation, Acta Metall. Mater., 34, 2259–2271, 1986.
Drury, M. R. and Humphreys, F. J.: Deformation lamellae as indicator of stress level, EOS T. Am. Geophys. Un., 44, 1471–1472, 1987.
Dunlap, W. J., Hirth, G., and Teyssier, C.: Thermomechanical evolution of a ductile duplex, Tectonics, 16, 983–1000, 1997.
Durinck, J., Devincre, B., Kubin, L., and Cordier, P.: Modeling the plastic deformation of olivine by dislocation dynamics simulations, Am. Mineral., 92, 1346–1357, 2007.
Ellis, S. and Stöckhert, B.: Elevated stresses and creep rates beneath the brittle-ductile transition caused by seismic faulting in the upper crust, J. Geophys. Res., 109, B05407, doi:10.1029/2003JB002744, 2004.
Evans, B. and Kohlstedt, D. L.: Rheology of rocks, in: Rock Physics and Phase Relations – a Handbook of Physical Constants, edited by: Ahrens, T. J., Ref. Shelf, 3, Am. Geophys. Union, 148–165, 1995.
Fredrich, J. T., Evans, B., and Wong, T.-F.: Micromechanics of the brittle to plastic transition in Carrata marble, J. Geophys. Res., 94, 4129–4145, 1989.
Heilbronner, R. and Tullis, J.: The effect of static annealing on microstructures and crystallographic preferred orientations of quartzites experimentally deformed in axial compression and shear, in: Deformation Mechanisms, Rheology and Tectonics: Current Status and Future Perspectives, Special Publications, 200, edited by: de Meer, S., Drury, M. R., de Bresser, J. H. P., and Pennock, G. M., Geological Society, London, 191–218, 2002.
Hirth, G. and Tullis, J.: Dislocation creep regimes in quartz aggregates, J. Struct. Geol., 14, 145–159, 1992.
Hirth, G. and Tullis, J.: The brittle-plastic transition in experimentally deformed quartz aggregates, J. Geophys. Res., 99, 731–748, 1994.
Hirth, G., Teyssier, C., and Dunlap, W. J.: An evaluation of quartzite flow laws based on comparisons between experimentally and naturally deformed rocks, Int. J. Earth Sci., 90, 77–87, 2001.
Hobbs, B. E.: Recrystallization of single crystals of quartz, Tectonophysics, 6, 353–401, 1968.

SED
5, 281–314, 2013

Hobbs, B. E.: The geological significance of microfabric analysis, in: Preferred Orientation in Deformed Metals and Rocks: an Introduction to Modern Texture Analysis, edited by: Wenk, H.-R., Academic Press, Orlando, Florida, 463–484, 1985.
Humphreys, F. J. and Hatherly, M.: Recrystallization and Related Annealing Phenomena, Elsevier Ltd., Oxford, 2004.
Karato, S.-I.: Deformation of Earth Materials: an Introduction to the Rheology of Solid Earth, Cambridge University Press, Cambridge, 2008.
Kruhl, J. H.: Prism- and basis-parallel subgrain boundaries in quartz: a micro-structural geothermobarometer, J. Metamorph. Geol., 14, 581–589, 1996.
Küster, M. and Stöckhert, B.: High differential stress and sublithostatic pore fluid pressure in the ductile regime – microstructural evidence for short term postseismic creep in the Sesia Zone, Western Alps, Tectonophysics, 303, 263–277, 1999.
Le, K. C., Korobeinik, M., and Hackl, K.: Estimation of crack density due to fragmentation of brittle ellipsoidal inhomogeneities embedded in a ductile matrix, Arch. Appl. Mech., 74, 439–448, 2005.
Matysiak, A. K. and Trepmann, C. A.: Crystal-plastic deformation and recrystallization of peridotite controlled by the seismic cycle, Tectonophysics, 530–531, 111–127, 2012.
McLaren, A. C.: Transmission Electron Microscopy of Minerals and Rocks, Cambridge University Press, New York, 1991.
McLaren, A. C. and Hobbs, B. E.: Transmission electron microscope investigation of some naturally deformed quartzites, in: Flow and Fracture of Rocks, Geophys. Monogr. 16, edited by: Heard, H. C., Borg, I. Y., Carter, N. C., and Raleigh, C. B., Am. Geophys. Union, 55–66, 1972.
McLaren, A. C., Turner, R. G., and Boland, J. N.: Dislocation structure of the deformation lamellae in synthetic quart, a study by electron and optical microscopy, Contrib. Mineral. Petr., 29, 101–115, 1970.
Nicolas, A. and Poirier, J. P.: Crystalline Plasticity and Solid State Flow in Metamorphic Rocks, Wiley-Interscience, London, 1976.
Nüchter, J. A. and Ellis, S.: Complex states of stress during the normal faulting seismic cycle: role of midcrustal postseismic creep, J. Geophys. Res., 115, B12411, doi:10.1029/2010JB007557, 2010.

SED
5, 281–314, 2013

Nüchter, J. A. and Stöckhert, B.: Vein quartz microfabrics indicating progressive evolution of fractures into cavities during postseismic creep in the middle crust, J. Struct. Geol., 29, 1445–1462, 2007.
Passchier, C. W. and Trouw, R. A. J.: Microtectonics, 2nd Edn., Springer Verlag, Berlin Heidelberg New York, 2008.
Paterson, M. S.: The ductility of rocks, in: Physics of Strenght and Plasticity, edited by: Argon, A. S., MIT Press, Cambridge, MA, 377–392, 1969.
Paterson, M. S.: Problems in the extrapolation of laboratory rheological data, Tectonophysics, 133, 33–43, 1987.
Paterson, M. S.: Rock deformation experimentation, Geoph. Monog. Series, 56, 187–194, 1990.
Paterson, M. S. and Wong, T.-F.: Experimental Rock Deformation – the Brittle Field, 2nd Edn., Springer-Verlag, Berlin Heidelberg, 2005.
Rybacki, E., Renner, J., Konrad, K., Harbott, W., Rummel, F., and Stöckhert, B.: a servohydraulically-controlled deformation apparatus for rock deformation under conditions of ultra-high pressure metamorphism, Pure Appl. Geophys., 152, 579–606, 1998.
Schmid, S. and Casey, M.: Complete fabric analysis of some commonly observed quartz c-axis patterns, Geophy. Monog. Series, 36, 263–286, 1986.
Scholz, C. H.: The Mechanics of Earthquakes and Faulting, 2nd ed., Cambridge University Press, Cambridge, 2002.
Stipp, M. and Kunze, K.: Dynamic recrystallization near the brittle-plastic transition in naturally and experimentally deformed quartz aggregates, Tectonophysics, 448, 77–97, 2008.
Stipp, M., Tullis, J., Scherwath, M., and Behrmann, J. H.: a new perspective on paleopiezometry: dynamically recrystallized grain size distributions indicate mechanism changes, Geology, 38, 759–762, 2010.
Stöckhert, B., Brix, M. R., Kleinschrodt, R., Huford, A. J., and Wirth, R.: Thermochronometry and microstructures of quartz – a comparison with experimental flow laws and predictions on the temperature of the brittle-plastic-transition, J. Struct. Geol., 21, 351–369, 1999.
Stünitz, H., Fitz Gerald, J. D., and Tullis, J.: Dislocation generation, slip systems, and dynamic recrystallization in experimentally deformed plagioclase single crystals, Tectonophysics, 372, 215–233, 2003.

SED
5, 281–314, 2013

Tonge, A. L., Kimberley, J., and Ramesh, K. T.: The mechanism of compressive unloading failure in single crystal quartz and other brittle solids, Int. J. Solids Struct., 49, 3923–3934, 2012.
Trepmann, C. A.: Shock effects and pre-shock microstructures in hydrothermal quartz veins from the Rochechouart impact structure, France, J. Struct. Geol., 31, 1183–1196, 2009.
Trepmann, C. and Stöckhert, B.: Mechanical twinning of jadeite – an indication of synseismic loading beneath the brittle-ductile transition, Int. J. Earth Sci., 90, 4–13, 2001.
Trepmann, C. A. and Stöckhert, B.: Cataclastic deformation of garnet: a record of synseismic loading and postseismic creep, J. Struct. Geol., 24, 1845–1856, 2002.
Trepmann, C. A. and Stöckhert, B.: Quartz microstructures developed during non-steady state plastic flow at rapidly decaying stress and strain rate, J. Struct. Geol., 25, 2035–2051, 2003.
Trepmann, C. A., Stöckhert, B., Dorner, D., Küster, M., Röller, K., and Hamidzadeh Moghadam, R.: Simulating coseismic deformation of quartz in the middle crust and fabric evolution during postseismic stress relaxation – an experimental study, Tectonophysics, 442, 83–104, 2007.
Trimby, P. W., Prior, D. J., and Wheeler, J.: Grain boundary hierarchy development in a quartz mylonite, J. Struct. Geol., 20, 917–935, 1998.
Tse, S. T. and Rice, J. R.: Crustal earthquake instability in relation to the depth variation of frictional slip properties, J. Geophys. Res., 91, 9452–9472, 1986.
Tsenn, M.-C. and Carter, N.-L.: Upper limits of power law creep of rocks, Tectonophysics, 136, 1–26, 1987.
Van Daalen, M., Heilbronner, R., and Kunze, K.: Orientation analysis of localized shear deformation in quartz fibres at the brittle-ductile transformation, Tectonophysics, 303, 83–107, 1999.
Vernooij, M. G. C., Kunze, K., and den Brok, B.: "Brittle" shear zones in experimentlly deformed quartz single crystals, J. Struct. Geol., 28, 1292–1306, 2006.
White, S.: Deformation lamellae in naturally deformed quartz, Nat. Phys. Sci., 245, 26–28, 1973.
White, S.: The effects of polyphase deformation on the intracrystalline defect structures of quartz, II. Origin of the defect structures, Neues Jb. Miner. Abh., 123, 237–252, 1975.
White, S. and Treagus, J. E.: The effects of polyphase deformation on the intracrystalline defect structures of quartz, I. The defect structures, Neues Jb. Miner. Abh., 123, 219–236, 1975.

SED
5, 281–314, 2013

Wilkins, R. W. T. and Barkas, J. P.: Fluid inclusions, deformation and recrystallisation in granite tectonites, Contrib. Mineral. Petr., 65, 293–299, 1978.

SED
5, 281–314, 2013

Table 1. Experimental data.

Sample	High-stress deformation "Kick"						Low-stress deformation at high temperature "Creep"						
	$P_{conf.}$ [GPa]	$T_{nom.}$ [°C]	$T_{meas.}$ [°C]	$d\varepsilon/dt$ [s^{-1}]	$\Delta\sigma_{max.}$ [GPa]	ε_1 [%]	$P_{conf.}$ [GPa]	$T_{nom.}$ [°C]	$T_{meas.}$ [°C]	$d\varepsilon/dt$ [s^{-1}]	$\Delta\sigma_{max.}$ [MPa]	$\varepsilon_{tot} - \varepsilon_1$ [%]	ε_{tot} [%]
CR1-1	2	400	**400**	$\mathbf{10^{-4}}$	3.3	2	–	–		–	–		2
CR1-3	2	400	396	$\mathbf{10^{-4}}$	3.2	2	–	–		–	–		2
CR1-13	2	400	402	$\mathbf{10^{-4}}$	3.4	3	2.5	900	913	1.8×10^{-6}	254	10	13
CR1-14	2	400	*	$\mathbf{10^{-4}}$	3.2	2	2.5	950	*	0.5×10^{-6}	140	2.5	4.5
CR1-15	2	400	*	$\mathbf{10^{-4}}$	1.2	< 1	2.7	1000	*	1.1×10^{-6}	152	~ 6	6.5
CR1-16	2	400	375	$\mathbf{10^{-4}}$	3.0	n.n.	2.5	900	860	0.2×10^{-6}	125	~ 1	1.5
CR1-17	2	400	420	$\mathbf{10^{-4}}$	2.5	< 1	2.5	900	902	0.2×10^{-6}	125	~ 1	1.4

P_{conf}, $\Delta\sigma_{max}$, ε_1, and $d\varepsilon/dt$ denote confining pressure ($\sigma_2 = \sigma_3$), maximum differential stress attained, axial strain, and average strain rate, respectively. $T_{nom.}$ denotes nominal temperature read out at thermocouple used for controlling, and $T_{meas.}$ temperature measured at second thermocouple, which failed in two experiments (*). Temperatures are not corrected for pressure. In the creep stage of experiment CR1-13, the axial piston was moved into the sample assembly to hold the load approximately constant, whereas in the other "creep" experiments the piston was kept stationary and stresses decreased with time (Fig. 1). See text for details.

SED
5, 281–314, 2013

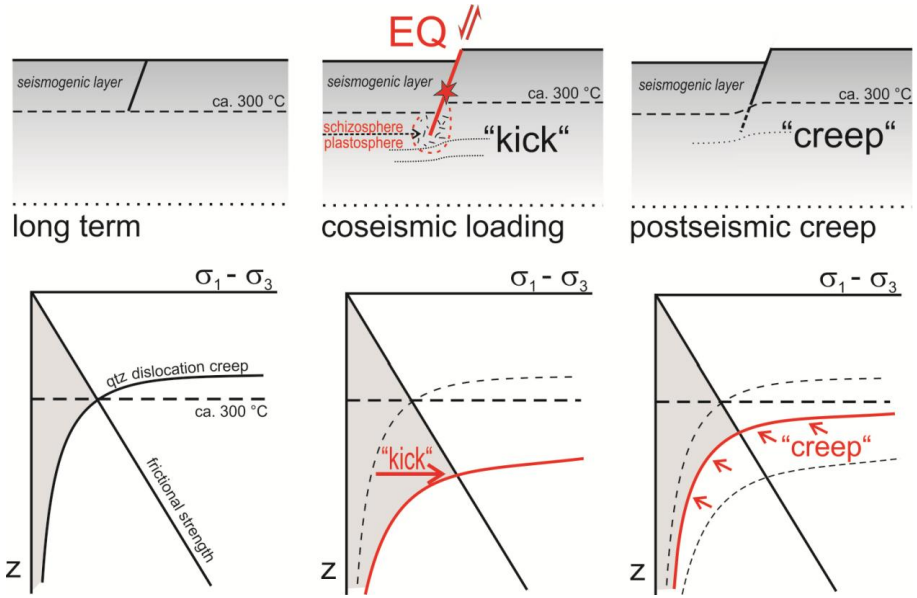

Fig. 1. Stress and strain rate changes during the seismic cycle, visualized by hypothetical crustal strength profiles (not to scale). Hypocenter is marked by asterisk. Around the lower termination of the downward propagating rupture plane of a large earthquake, i.e. at the boundary between schizosphere and plastosphere sensu Scholz (2002), quasi-instantaneous coseismic loading to high differential stress causes deformation of quartz in the low-temperature plasticity regime ("kick"). During subsequent stress relaxation and restoration of long-term state, quartz deforms by dislocation creep at decaying strain rate ("creep"), each stage of the earthquake-related stress cycle leaving a characteristic microstructural imprint. In the present study, modification of microstructures acquired during the "kick" stage in the course of subsequent "creep" deformation is investigated in laboratory experiments.

SED
5, 281–314, 2013

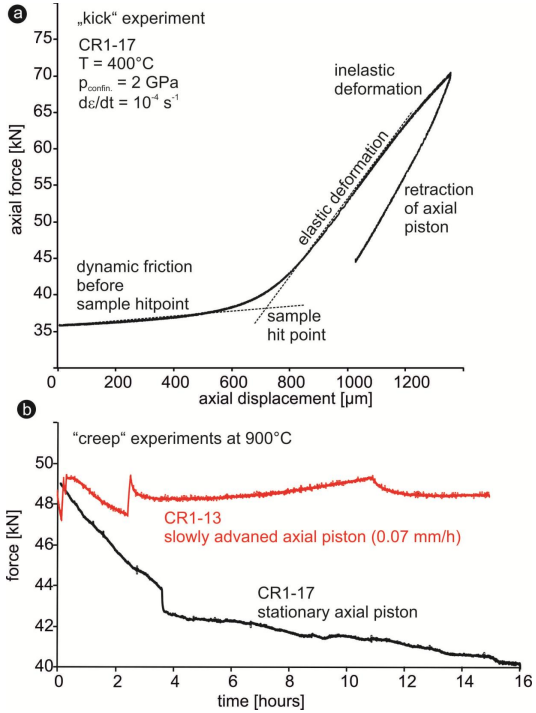

Fig. 2. Selected force-time curves for **(a)** low-temperature, high-stress “kick” experiment CR1-3, and for **(b)** high-temperature, low-stress (“creep”) stage in the experiments CR1-13 (stress kept approximately constant) and CR1-17 (stress relaxation).

SED
5, 281–314, 2013

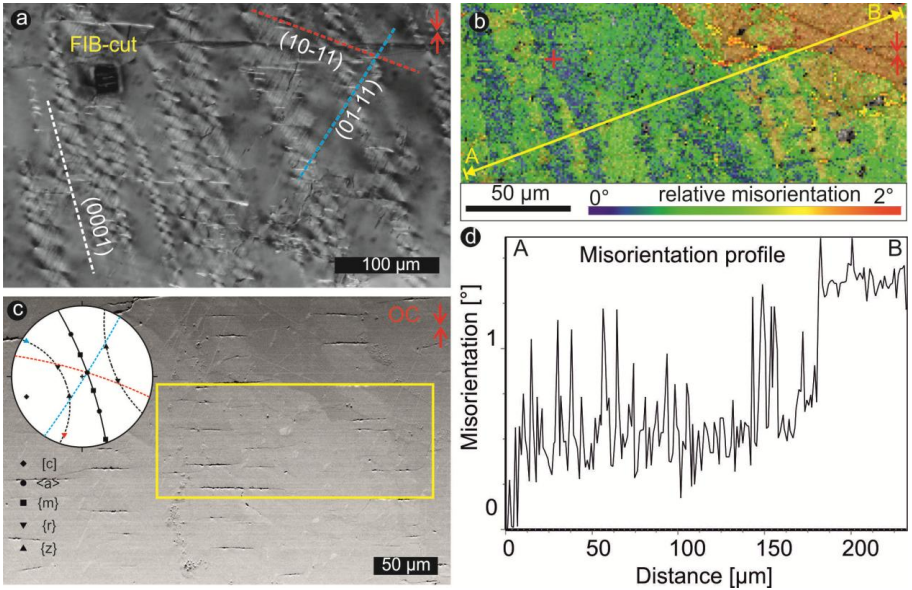

Fig. 3. Quartz microfabric from "kick" experiment CR-1-3 performed at 400 °C, 2 GPa confining pressure, and strain rate of 10^{-4} s^{-1}. The shortening direction is vertical in all images, indicated by red arrows. **(a)** Optical micrograph (crossed polarizers) showing slightly misoriented domains parallel (0001), containing arrays of microcracks and lamellae parallel to {r} and {z} rhombohedral planes. Location of FIB-prepared TEM foil is shown by a yellow rectangle. **(b)** EBSD map showing domains with misorientation relative to reference point (red cross); colors indicate misorientation, displayed as overlay on band contrast image in grey shades; non-colored areas are not indexed; yellow line indicates location of the misorientation profile shown in **(d)**. **(c)** Orientation contrast image of area shown in **(a)** and pole figure (lower hemisphere, equal angle) displaying crystallographic orientation. **(d)** Misorientation relative to point a along the yellow line displayed in **(b)**.

SED
5, 281–314, 2013

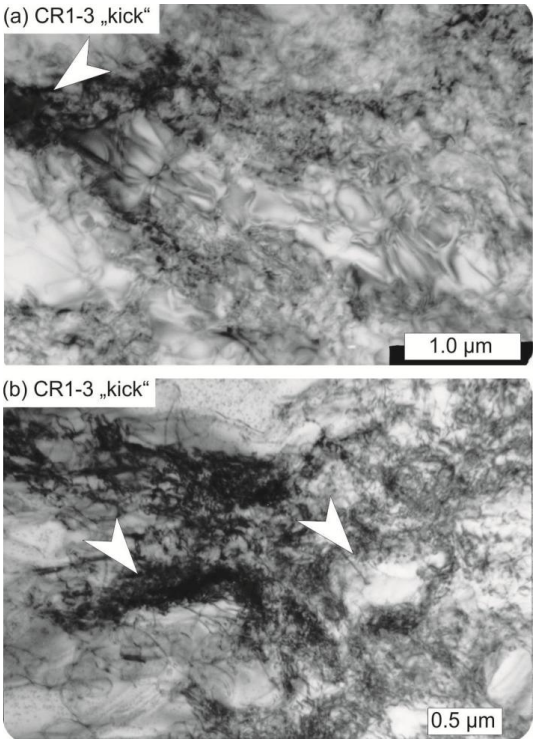

Fig. 4. TEM bright field micrographs of quartz from “kick” experiment CR-1-3 performed at 400 °C, 2 GPa confining pressure, and strain rate of 10^{-4} s^{-1}, being exceedingly prone to radiation damage. **(a, b)** TEM-micrographs from FIB cut foil located in Fig. 3a (“kick” experiment CR1-3). Quartz shows dislocation tangles and domains poor in dislocations bound by tangles and dislocation walls (arrows), resembling a cellular structure.

SED
5, 281–314, 2013

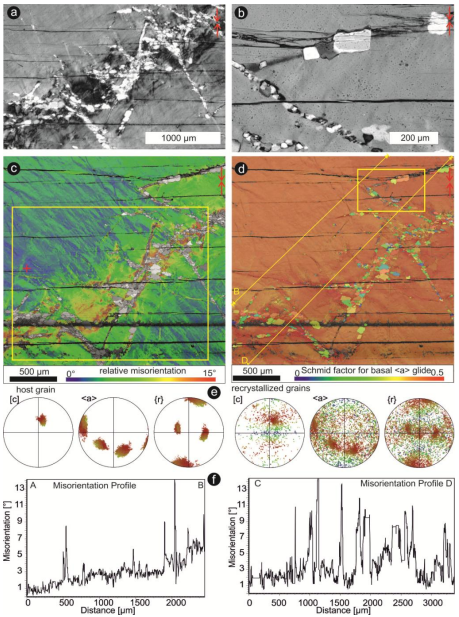

Fig. 5. Quartz microfabric from "kick and creep" experiment CR1-16, initially deformed at 400 °C, 2 GPa confining pressure, strain rate $10^{-4}\,s^{-1}$, and afterwards at 900 °C, 2.5 GPa confining pressure, undergoing stress relaxation. **(a, b)** Optical micrographs (crossed polarizers) showing bands of recrystallized grains and pronounced SWUE. **(c)** EBSD map showing misorientation relative to reference point (red cross); colors indicate misorientation, displayed as overlay on band contrast image in grey shades; non-colored areas are not indexed. **(d)** EBSD map showing Schmid factor for basal ⟨a⟩ glide. The yellow lines indicate location of misorientation profiles shown in **(f)**. **(e)** Pole figures showing crystallographic orientation of host grain and recrystallized grains, respectively. **(f)** Misorientation relative to first points (a and C) along yellow lines displayed in **(b)**.

SED
5, 281–314, 2013

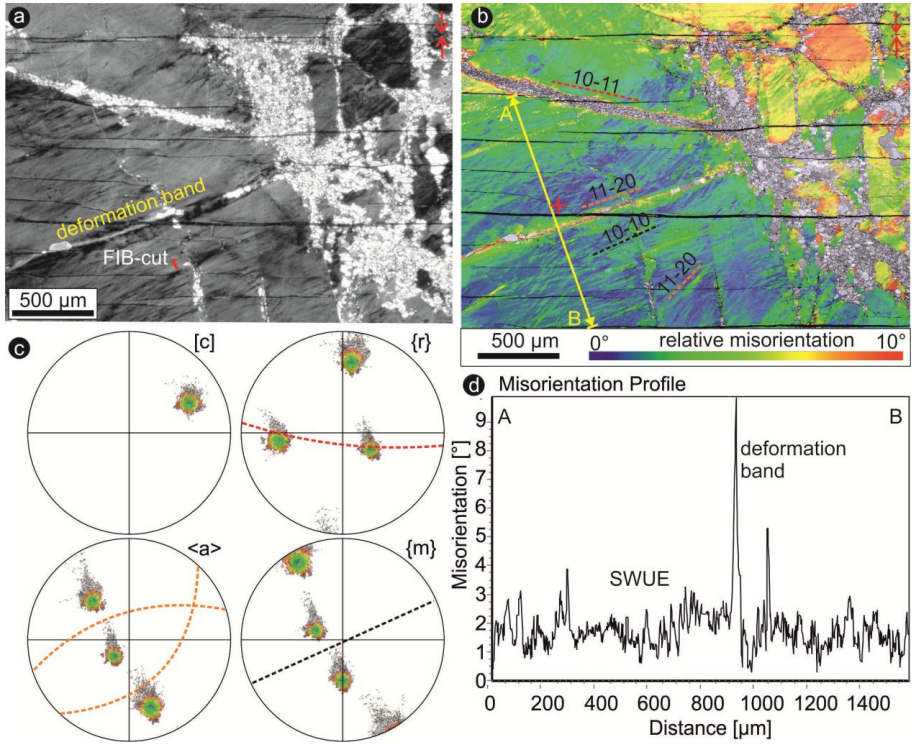

Fig. 6. Quartz microfabric from "kick and creep" experiment CR1-17, initially deformed at 400 °C, 2 GPa confining pressure, 10^{-4} s^{-1} strain rate, and afterwards at 900 °C, 2.5 GPa confining pressure and approximately constant stress. **(a)** Optical micrograph (crossed polarizers) showing strings of recrystallized grains, deformation bands and pervasive SWUE. Location of FIB cut TEM foil is marked by red rectangle. **(b)** EBSD map showing misorientation relative to reference point (red cross). Red line indicates location of misorientation profile displayed in **(f)**. **(c)** Pole figures showing crystallographic orientation of host grain. **(d)** Misorientation relative to point a along yellow line displayed in **(b)**.

SED
5, 281–314, 2013

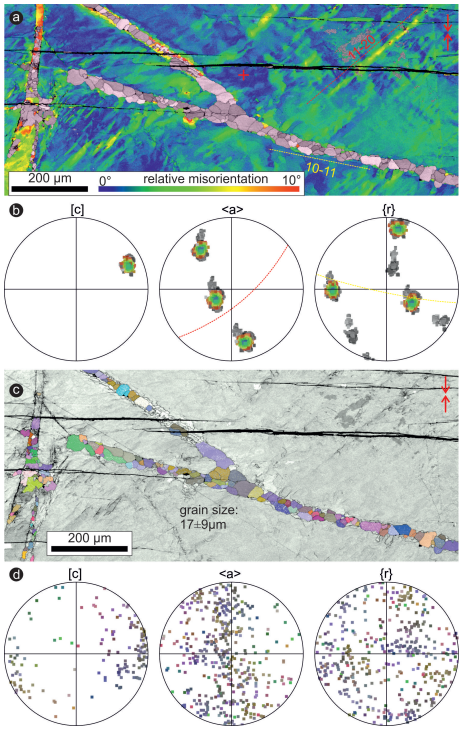

Fig. 7. SWUE and recrystallized quartz from "kick and creep" experiment CR1-17 initially deformed at 400 °C, 2 GPa confining pressure, 10^{-4} s^{-1} strain rate, and afterwards at 900 °C, 2.5 GPa confining pressure and approximately constant stress. **(a, b)** EBSD map showing misorientation relative to reference point marked by red cross and corresponding pole figures. Orientation of {a} prism and {r} rhombohedral planes are displayed as traces in EBSD map and as great circles in pole figures. **(c, d)** EBSD map showing new grains, colour coding corresponds to pole figures; crystallographic orientation of new grains is nearly random; orientation control by host grain is weak.

SED
5, 281–314, 2013

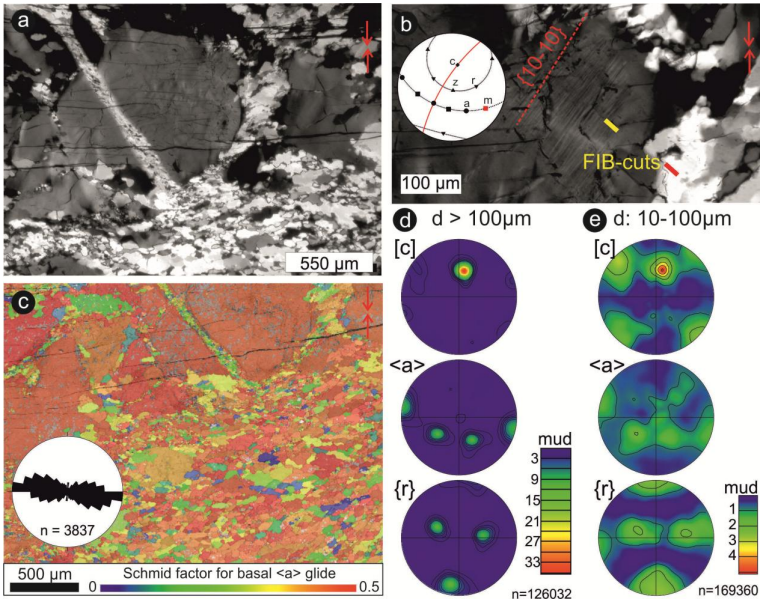

Fig. 8. Microfabric of quartz from "kick and creep" experiment CR1-13, initially deformed at 400 °C, 2 GPa confining pressure, and strain rate of 10^{-4} s^{-1}, and afterwards at 900 °C, 2.5 GPa confining pressure and approximately constant stress. **(a)** Optical micrograph showing partly recrystallized quartz. **(b)** Optical micrograph showing SWUE in large original quartz grain. **(c)** The yellow and red line are marking the location of FIB cut TEM foils, from which bright field images are shown in Fig. 9c,d. **(c)** EBSD-map showing Schmid factor for basal ⟨a⟩ glide by color code. **(d, e)** Pole figures (density plots) showing crystallographic orientation of grains with diameter larger than 100 µm and of grains with diameters of 10–100 µm.

SED
5, 281–314, 2013

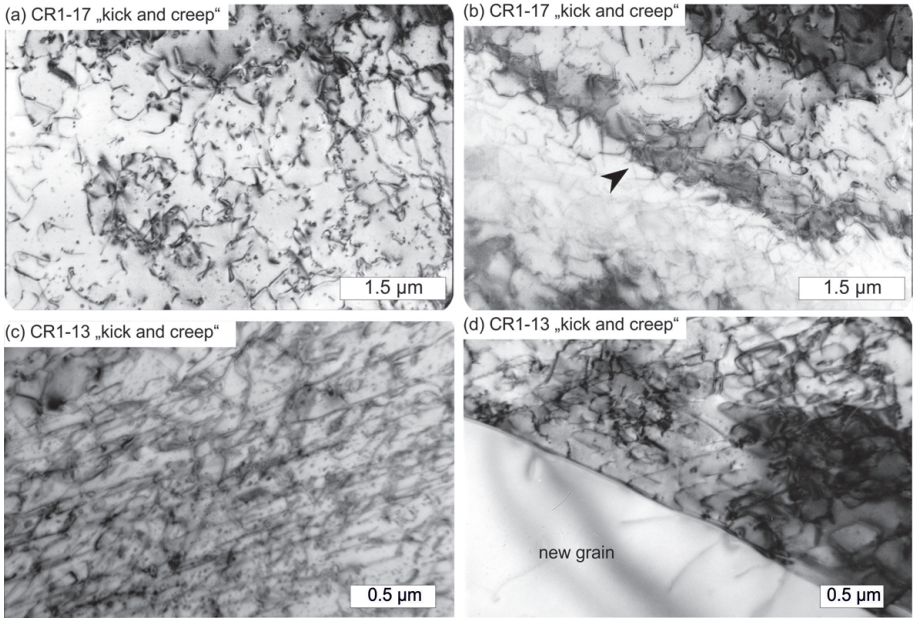

Fig. 9. TEM bright field micrographs of quartz, being exceedingly prone to radiation damage. **(a, b)** TEM-micrographs from FIB cut foils shown in Fig. 6c; “kick and creep” experiment CR1-17 with stress relaxation. Quartz shows dislocation density on the order of $10^{12}\,m^{-2}$. Poorly ordered dislocation wall in **(b)** is marked by arrow. **(c)** TEM-micrograph from FIB cut foil, location shown by yellow rectangle in Fig. 8b; “kick and creep” experiment CR1-13, with approximately constant stress. Quartz shows high density of dislocations arranged in walls parallel to optically visible SWUE. **(d)** TEM-micrograph from FIB cut foil located by red rectangle in Fig. 8b; “kick and creep” experiment CR1-13, with approximately constant stress; high angle grain boundary between deformed and recrystallized grain with low dislocation density.

SED
5, 281–314, 2013

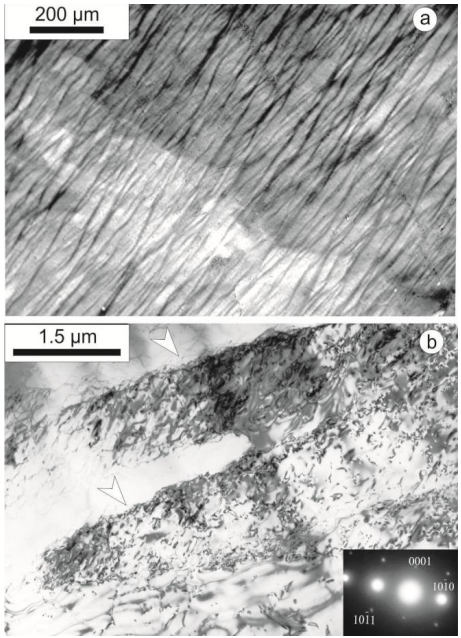

Fig. 10. Microstructures of naturally deformed vein quartz from St. Paul la Roche, France. **(a)** Optical micrograph showing pronounced SWUE. **(b)** TEM bright field micrographs of foil prepared by ion milling from region showing optical microstructure depicted in **(a)**. Poorly ordered dislocation walls (arrows) confine domains with a width of about 1 µm, where dislocations being in or out of contrast at slightly different tilt, indicating differing crystallographic orientation. Dislocation density is on the order of 10^{13} m^{-2}.

SED
5, 281–314, 2013

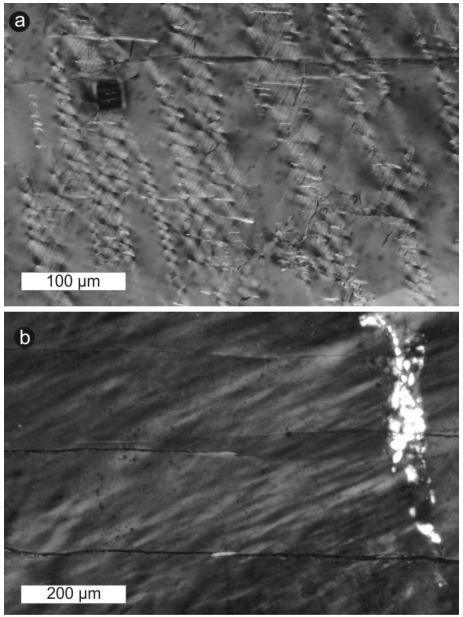

Fig. 11. Optical micrographs showing quartz microstructure after **(a)** "kick" experiment CR1-3 and **(b)** "kick and creep" experiment CR1-17. Note the different scale bar, which is chosen because of characteristically different wavelength of the microstructures. The microfabrics corresponding to **(a)** will not be observed in metamorphic rocks due to modification during prolonged cooling and exhumation history. Microfabrics depicted in **(b)** are similar to those found in exhumed metamorphic rocks (cf. Fig. 8) and indicate a stage of high stress deformation in the low-temperature plasticity field, probably related to large earthquakes (see text).

SED
5, 281–314, 2013